

ENGINEERING DESIGN OF LOW-EMITTANCE DC-SRF PHOTOCATHODE INJECTOR

Y. Q. Liu†, M. Chen, S. Huang, L. Lin, K. X. Liu, S. W. Quan, F. Wang, S. Zhao
Institute of Heavy Ion Physics, School of Physics, Peking University, Beijing, China

Abstract

An upgraded version of DC-SRF photocathode injector (DC-SRF-II) is under development at Peking University. The goal is to achieve an emittance below 0.5 mm-mrad at the bunch charge of 100 pC and repetition rate of 1 MHz. The engineering design of the DC-SRF-II photoinjector was accomplished in this May and the fabrication is ongoing now. This paper presents some details of the engineering design.

INTRODUCTION

Superconducting RF (SRF) photocathode injector has the advantage in principle to generate high average current, high-brightness electron beams and has been developed by several laboratories around the world [1-5]. To prevent the contamination of SRF cavity by the semiconductor photocathode materials, at Peking University, we have been developing a DC and SRF combined photocathode injector, known as the DC-SRF injector [6-8]. To meet the requirements of continuous-wave (CW) X-ray FELs, we are developing an upgraded DC-SRF photocathode injector (referred to as DC-SRF-II for short) with the goal to achieve an emittance below 0.5 mm-mrad at the bunch charge of 100 pC and repetition rate of 1 MHz. Recently, the engineering design of the new injector (which is shown in Fig. 1) has been finished and the fabrication is under way. In this paper, we present some results of the engineering design, including the redesign of the DC structure, the evaluation of thermal load for cryomodule, the design of magnetic shielding, and the evaluation of the mechanical property.

NEW DESIGN OF DC STRUCTURE

The DC structure of the injector has been redesigned according to our operation experience with the first-generation DC-SRF injector. The new design reduces the number of ceramics to two and provides a detachable protective electrode for the brazed position of ceramic and metal. Figure 2 shows the new DC structure. An inverted-geometry ceramic insulator approach was adopted. This insulator extends into the vacuum chamber serving as the cathode support structure. The advantage of this design is that it is compact and it helps to reduce field emission [9]. In addition, the shape of the high-voltage electrode was optimized, and the highest surface field has been controlled below 10 MV/m.

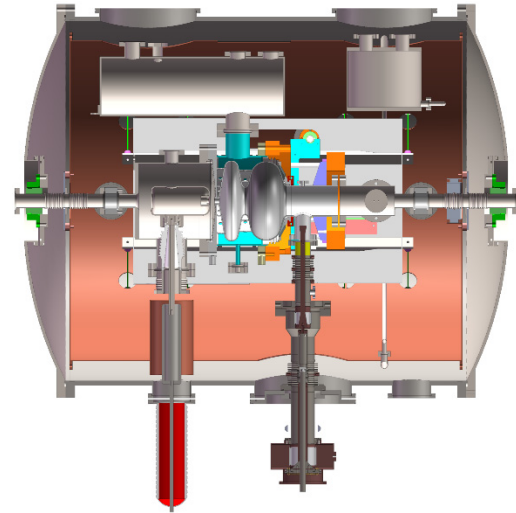


Figure 1: An overview of DC-SRF photocathode injector.

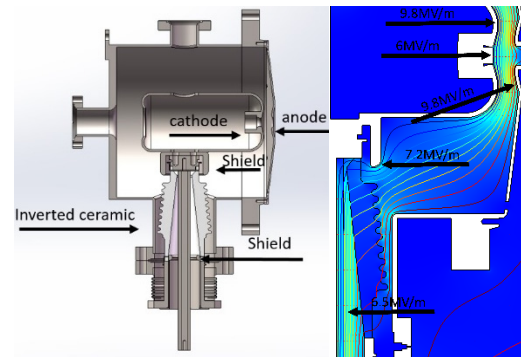


Figure 2: The new design of the DC structure (left) and electric field (right).

THERMAL EVALUATION OF THE CRYO-MODULE

The heat load of the cryomodule has been calculated via COMSOL Multiphysics [10]. Static heat load and dynamic heat load are shown in Table 1 and Table 2. The superconducting cavity surface loss can be estimated from the RF parameters in Table 3. The total heat load of cryomodule is about 12 W at 2 K and about 36 W at 77 K.

In addition, the flow direction of the liquid nitrogen pipe has been redesigned to obtain an optimized temperature distribution on the copper screen. Figure 3 shows that the highest temperature is about 87.5 K.

* Work supported by National Key Research and Development Program of China (Grant No. 2016YFA0401904).

† yqliu17@pku.edu.cn

Table 1: Static Heat Load Evaluation Results

Heat source	2 K / W	77 K / W
Power Coupler	0.4	4.9
Beam Line	0.2	2.1
Supported Rod	1.3	1.7
Tuner Rod	0.1	0.4
Radiation	0.5	10
Total	2.5	19.1

Table 2: Dynamic Heat Load Evaluation Results

Heat source	2 K / W	77 K / W
Power Coupler	1.1	16.2
1.5 Cell Cavity	8	\
Total	9.1	16.2

Table 3: RF Parameters of the Cavity

Parameter	Value	Unit
Frequency	1300	MHz
Q_0	1×10^{10}	\
E_{acc}	14	MV/m
Effective Length	186.6	mm
G-factor	212	Ω
Shunt Impedance r/Q	203	\
E_{peak}/E_{acc}	2.07	\
B_{peak}/E_{acc}	4.86	mT/(MV/m)

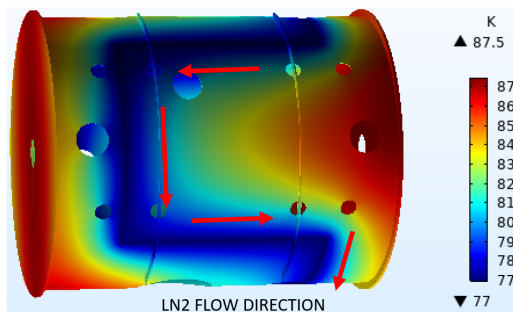


Figure 3: Temperature distribution of the 77 K copper screen.

MAGNETIC SHIELDING

The magnetic shield of the cryomodule consists an outer shell with 304 stainless steel and an inner shield with Permalloy. The goal is to shield the geomagnetic field (~0.5 Gs)

and the leakage field from the orbit corrector located 200 mm outside the Permalloy shield which is shown in Fig. 4. Figure 5 shows that with the shielding of Permalloy, the magnetic field around cavity is controlled below 10 mGs.

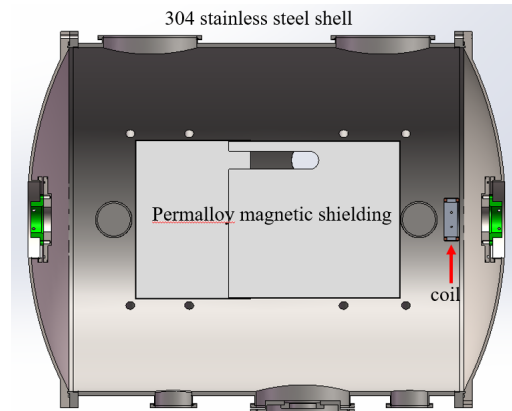


Figure 4: A layout of the magnetic shielding.

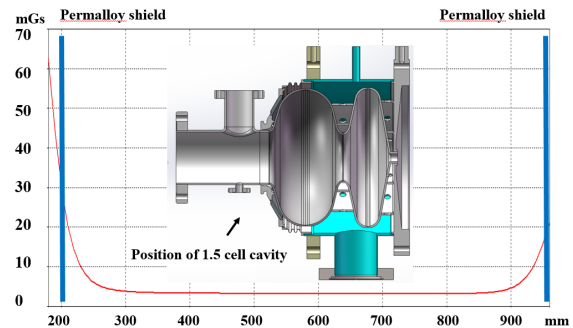


Figure 5: Effect of magnetic shielding.

MECHANICAL PROPERTIES OF THE INJECTOR

The variation of the field distribution and cavity frequency under the tuning forces are shown in Fig. 6. It takes about 35 kN to compress the cavity by 1 mm which leads a frequency change of 1.06 MHz. During the cooling process the frequency is supposed to increase about 2.8 MHz.

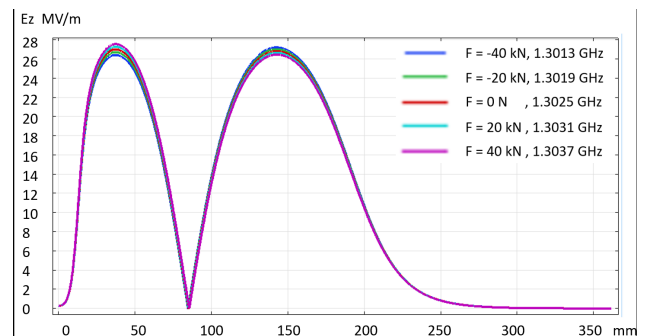


Figure 6: The effect of tuning on field flatness and frequency.

In addition, for gradient $E_{\text{acc}} = 14$ MV/m and tuner stiffness 35 kN/mm, the frequency shift due to Lorentz forces is supposed to be 555 Hz. For liquid helium pressure of 30 mbar the frequency shift is supposed to be 1.56 kHz. The evaluation results of mechanical parameters can be seen as Table 4.

Table 4: Mechanical Parameters Evaluation Results of Cavity

Parameter	Value	77 K / W
Frequency	1.3	GHz
Cool down	9.4	kHz/K
df/dp	42.6	Hz/mbar
LFD	-2.47	Hz/(MV/m) ²

CONCLUSION

The major changes include the redesign of the DC structure, the magnetic shielding, the RF coupler, and the cryostat. The engineering design has been accomplished and some results are shown in this paper.

REFERENCES

- [1] I. Petrushina *et al.*, “Novel Aspects of Beam Dynamics in CeC SRF Gun and SRF Accelerator”, in *Proc. FEL'17*, Santa Fe, NM, USA, Aug. 2017, pp. 313-316. doi:10.18429/JACoW-FEL2017-TUP034
- [2] A. Neumann *et al.*, “The BERLinPro SRF Photoinjector System - From First RF Commissioning to First Beam”, in *Proc. IPAC'18*, Vancouver, Canada, Apr.-May 2018, pp. 1660-1663. doi:10.18429/JACoW-IPAC2018-TUPML053
- [3] T. Konomi *et al.*, “Design and Fabrication of KEK Superconducting RF Gun #2”, in *Proc. LINAC'18*, Beijing, China, Sep. 2018, pp. 510-512. doi:10.18429/JACoW-LINAC2018-TUP0074
- [4] R. Xiang *et al.*, “Tuning Status of SRF Gun II at the ELBE Radiation Center”, in *Proc. LINAC'18*, Beijing, China, Sep. 2018, pp. 952-954. doi:10.18429/JACoW-LINAC2018-THP0125
- [5] E. Vogel *et al.*, “SRF Gun Development at DESY”, in *Proc. LINAC'18*, Beijing, China, Sep. 2018, pp. 105-108. doi:10.18429/JACoW-LINAC2018-MOP0037
- [6] K. Zhao *et al.*, “Research on DC-RF superconducting photocathode injector for high average power FELs”, *Nucl. Instr. and Meth. A*, vol. 475 (2001), p. 568. doi:10.1016/S0168-9002(01)01594-7
- [7] J. Hao *et al.*, “Primary beam-loading tests on DC-SC photoinjector at Peking University”, *Nucl. Instr. and Meth. A*, vol. 557 (2006), p. 141. doi:10.1016/j.nima.2005.10.063
- [8] S. Quan *et al.*, “Stable operation of the DC-SRF photoinjector”, *Nucl. Instr. and Meth. A*, vol. 798 (2015), p. 117-120. doi:10.1016/j.nima.2015.07.025
- [9] Y. W. Wang *et al.*, “300 kV DC High Voltage Photogun with Inverted Insulator Geometry and CsK2sb Photocathode”, in *Proc. IPAC'18*, Vancouver, Canada, Apr.-May 2018, pp. 4571-4574. doi:10.18429/JACoW-IPAC2018-THPMK110
- [10] COMSOL, <http://cn.comsol.com>